JOURNAL OF Applied Polymer SCIENCE

Orientation Microstructure and Properties of Poly(propylene carbonate)/poly(butylene succinate) Blend Films

G. J. Chen, Y. Y. Wang, S. J. Wang, M. Xiao, Y. Z. Meng

The Key Laboratory of Low-carbon Chemistry & Energy Conservation of Guangdong Province, State Key Laboratory of Optoelectronic Materials and Technologies, Sun Yat-sen University, Guangzhou 510275, People's Republic of China

Correspondence to: Y. Z. Meng (E-mail: mengyzh@mail.sysu.edu.cn) or M. Xiao (E-mail: stsxm@mail.sysu.edu.cn)

ABSTRACT: The blends of high molecular weight poly(propylene carbonate) (PPC) and poly(butylene succinate) (PBS) were melt blended using triphenylmethane triisocyanate (TTI) as a reactive coupling agent. TTI also serves as a compatibilizer for the blends of PPC and PBS. The blend containing 0.36 wt % TTI showed that the optimal mechanical properties were, therefore, calendared into films with different degrees of orientation. The calendering condition, degree of orientation, morphologies, mechanical properties, crystallization, and thermal behaviors of the films were investigated using wide-angle X-ray diffraction, scanning electron microscopy, tensile testing, and differential scanning calorimetry (DSC) techniques. The result showed that the as-made films exhibited obvious orientation in machine direction (MD). Both tensile strength in MD and the tear strength in transverse direction (TD) increased with increasing the degree of orientation. The orientation of the film also increased the crystallinity and improved the thermal properties of the PPC/PBS blend films. © 2012 Wiley Periodicals, Inc. J. Appl. Polym. Sci. 000: 000–000, 2012

KEYWORDS: poly(propylene carbonate); poly(butylene succinate); triphenylmethane triisocyanate; calendared film

Received 22 February 2012; accepted 31 May 2012; published online
DOI: 10.1002/app.38150

INTRODUCTION

The development of plastics industry had serious consequences for the environment, called "White Pollution,"[1] because of their not biodegradability. In recent years, much attention has been paid to aliphatic polyesters; they show good biodegradability and excellent comprehensive performance. For instance, poly (lactic acid) (PLA), poly(3-hydroxybutyrate-*co*-3-hydroxyvalerate), and poly(butylene succinate) (PBS) are the outstanding representatives of them.[2–8] Moreover, the mass emission of CO_2 produced by industries is believed to cause the global warming that may contribute to the climate change.[9–11] On the other hand, the utilization of CO_2 as resource has attracted more and more researcher of late years; the copolymerization of CO_2 with epoxide to form biodegradable aliphatic polycarbonate is one of the promising ways.[12–16] The fixation of CO_2 in the synthesis of biodegradable polycarbonate not only eases dependence on petroleum but also reduces the massive emission of CO_2, which can mitigate the greenhouse effect.

In previous works, high molecular weight poly(propylene carbonate) (PPC; $M_n > 250{,}000$) has been successfully synthesized from CO_2 and PO using supported catalyst under optimized reaction conditions, and alternating PPC in very high yields (126 g of polymer per gram catalyst) has also been synthesized successfully in our laboratory.[17–19] PPC with alternating molecular structure exhibits fairish mechanical properties and considerable degradability in surroundings of both soil and buffer solutions. However, poor thermal properties limit its practical application areas.

PPC possesses many particular characteristics. Its amorphous nature can endow many unique properties, such as highly oxygen barrier property. On the other hand, to produce PPC-based films, it is very important to improve its melt and static strength.[20–24] PBS is aliphatic polyester with semicrystalline structure and biodegradable nature. Because of its high crystallinity and crystalline structure, it exhibits excellent mechanical properties and thermal stability.[7,25] In our previous work, we reported the miscibility and properties of PPC/PBS blends.[26] The compatibility between PPC and PBS can be effectively improved by simple melt compounding in the presence of compound containing reactive groups. Both PPC and PBS have terminated hydroxyl groups, which can then react with isocyanates to enhance the comprehensive properties of PPC/PBS blends (Figure 1). Numerous works using isocyanates as reactive agent have been reported.[27,28] For example, Zeng et al.[29] used toluene diisocyanate as chain extender to synthesize multiblock poly(ester urethane), consisting of poly(L-lactic acid) and PBS blocks; Harada[30] prepared PLA/PBS blends using lysine

Applied Polymer SCIENCE

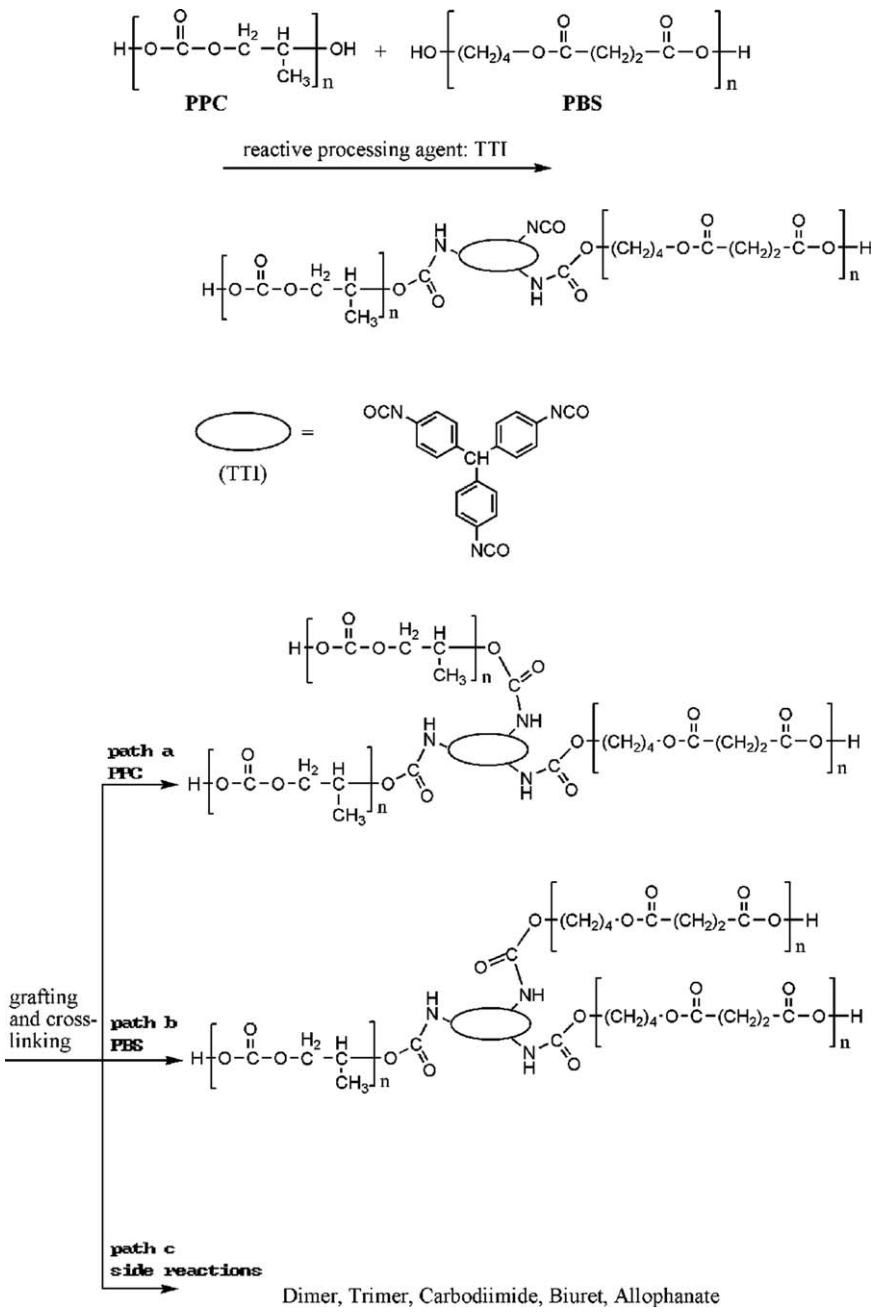

Figure 1. Reaction scheme of PPC, PBS, and TTI.

triisocyanate (LTI) and lysine diisocyanate (LDI), and they found that the blends with LTI exhibited much better physical properties than that with LDI.

In this work, PPC was blended with PBS in the presence of triphenylmethane triisocyanate (TTI) in a twin-screw extruder. The film from the as-made PPC/PBS blends with TTI as reactive agent was then prepared using a single extruder connected to a calendar. Finally, the orientated films were obtained, and the morphology, crystallinity, and mechanical properties of the films were investigated by different techniques.

Diphenyl-methane-diisocyanate (MDI) was also used in this work to compare the effectiveness with TTI. We found that TTI exhibits much effectively compared with MDI when considering the mechanical and thermal properties of the blends.

The novelties of this work are as follows: (1) TTI was used as reactive agent for the coupling reaction between PBS and a new copolymer of PPC and (2) the calendared film of PPC/PBS blends was prepared and reported for the first time.

EXPERIMENTAL

Materials

The high molecular weight PPC [melt flow rate (MFR) (170°C, 2.16 kg) = 13.2 g/10 min], with a number-average molecular weight (M_n) of 125,000 Da and a polydispersity (PD) of 1.91,

Table I. Temperature Profiles of Twin-Screw Extruder

Section	#1	#2	#3	#4	#5	Die
Temperature (°C)	165	175	180	185	185	180

Table II. Temperature Profiles of Single-Screw Extruder

Section	#1	#2	#3	Die
Temperature (°C)	175	180	185	160–210

was supplied by Tianguan Enterprise Group (Henan, China). PBS [M_n = 64,000 Da, PD = 2.27, melting temperature (T_m) = 115°C, MFR (170°C, 2.16 kg) = 2.4 g/10 min] was obtained from Hangzhou Hemao Polymers (Hangzhou, China) in pellet form. Triphenylmethane-4,4′,4″-triisocyanate (TTI) was provided by Hengbang Chemical Engineering (Changzhou, China). PPC and PBS pellets were dried in a vacuum oven for 24 h at 80°C before blending.

Blending

PPC, PBS, and TTI were melt compounded into pellets in a corotating twin-screw extruder (diameter = 50 mm, L/D = 40 : 1) at 100 rpm, and the temperature distribution is tabulated in Table I. Different weight ratios of PPC and PBS to TTI were mechanically mixed well in a high-speed mixer before melt blending.

Film Calendaring

The calendared films were prepared by a single-screw extruder (diameter = 20 mm, L/D = 25) which is attached to the calendar die (width = 200 mm, gap thickness = 0.2 mm) and an I-type three-roller calendar device. The profile of the calendar device is shown in Figure 2. In this work, all the three rollers and the winder were kept the same linear speed; the rollers were cooled by running water, the blend melt came out from the die in sheet form, and then it became film after passing through the gap of following two rollers. The produced film was cooled down through the top roller followed by rolling up.

When calendared, the die temperature ranged from 160 to 210°C (Table II), and the screw speed was set to be 70 rpm. Mechanical properties of the films were examined to monitor and find out the optimal experimental conditions. Consequently, the die temperature was selected to be 200°C, the screw speed of single-screw extruder be 70 rpm, and calendar's roller speed be from 15 to 35 rpm.

MFR

The MFR of PPC/PBS blends were measured using a MFR tester (MC-400C, Taiwan, China) at standard conditions of 170°C and 2.16 kg nominal load according to ASTM D 1238-82 standard.

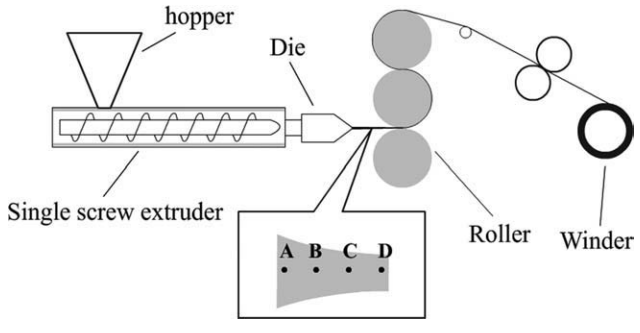

Figure 2. The schematic illustration of film calendaring.

Vicat Softening Point

The vicat softening point of the blends was measured using a vicat tester (New SANS, Shenzhen, China) at 10 N load and heating rate 50°C/h. The test was performed according to ASTM D 1525. Six specimens have been examined for each type of blends, and average value was reported accordingly.

Tensile Strength

100 × 15 mm^2 rectangle samples were cut from the films for tensile tests. The tensile tests were performed using a temperature-controlled tensile tester (New SANS, Shenzhen, China) at 25°C with a relative humidity of 50 ± 5%. The crosshead speed of the dumb-bell bars was set at 50 mm/min, whereas that of rectangle samples was 20 mm/min. Five specimens of each sample were tested, and the average results were recorded.

Tear Strength

The Graves tear strength of the films was measured according to ASTM D 1004. The crosshead speed was set at 51 mm/min.

Essential Work of Fracture

The essential work of fracture was first suggested by Broberg,[31,32] and later developed by Cotterell, Mai, and their coworkers[33–40] on polymers and polymer films.

For the fracture of a precracked specimen, the total fracture work (W_f) can be separated into the essential work of fracture (W_e) and the nonessential (plastic) work (W_p). Thus, the total fracture work can be written as:

$$W_f = W_e + W_p. \quad (1)$$

W_e and W_p are responding to the inner fracture process zone and the outer plastic zone. The essential work of fracture represents the work at the end region in the vicinity of the crack tip that initiates the crack. The nonessential work of fracture represents the work at the outer region that is responsible for the plastic deformation of the material following crack initiation and propagation.

According to the essential work of fracture (EWF) concept, W_e is essentially a surface energy; it is proportional to the ligament length l (for a given specimen thickness). W_p is a volume energy, which is proportional to l^2 (also for a given specimen thickness). So, the result is the following equation:

$$w_f = W_f/lt = w_e + l\beta w_p. \quad (2)$$

where w_f, w_e, and w_p are the specific total fracture work, specific essential work of fracture, and specific plastic work, respectively. t is the specimen thickness and β is the plastic zone shape factor.

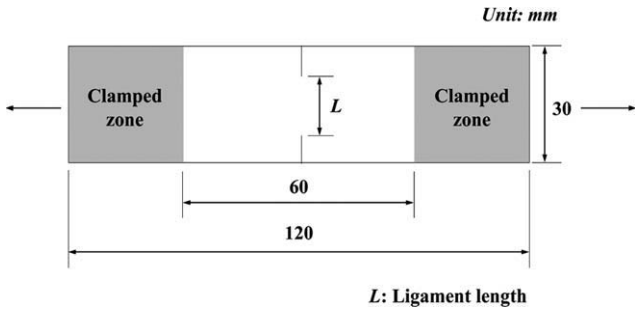

Figure 3. Specimen geometry of EWF test.

It can be found that there is a linear relationship between the specific work of fracture (w_f) and ligament length (l). If we plot w_f versus l, the specific essential work of fracture (w_e), and the specific inessential work (βw_p) can be obtained.

For the valid measurement of plane stress w_e, the ligament l has to satisfy the following equation:

$$(3-5)t \le l \le \min(W/3 \text{ or } 2r_p). \tag{3}$$

where W is the width of the specimen, t is specimen thickness, and r_p is size of the plastic zone.

In this study, four different ligament sizes were selected (3, 5, 7, and 9 mm), and three specimens were tested for each ligament length. The geometry of the test specimen is shown in Figure 3. The EWF test is designed to correlate the tear property as measured by the Graves tear test; therefore, the test speed was selected as 51 mm/min. The test temperature was 25°C.

Differential Scanning Calorimetry Investigation

The samples were scanned with differential scanning calorimetry (DSC; Netzsch 204, Burlington, Germany). To investigate the thermal properties of the films, the temperature was initially cooled from room temperature to −25°C at a rate of 10°C/min, maintained at −25°C for a period of 3 min, and then increased to 150 at 10°C/min. All the scanning processes were under a protective atmosphere of N_2.

Wide-Angle X-Ray Diffraction

Wide-angle X-ray diffraction (WAXD) measurements were performed with an X-ray diffractometer (D/Max-IIIA, Rigaku, Japan) at a scanning speed of 5°/min with a 2θ range of 5–40°. The X-ray source was a 3-kW rotating anode X-ray generator equipped with a rotating anode Cu target. Radial scans for specific 2θ were obtained by fixing 2θ and changing the azimuthal angles ϕ from −90 to 90° (equator being 0°) with a rotating sample holder at a rotating speed of 60°/min.

The degree of orientation of crystalline regions can be calculated using the Hermans–Stein orientation function,[41]

$$f_c = \frac{3\langle\cos^2\phi_{c,Z}\rangle - 1}{2} \tag{4}$$

f_c is the Hermans–Stein orientation parameter, and $\phi_{c,z}$ is the angle between the c crystal axis and the drawing direction. $\langle\cos^2\phi_{c,Z}\rangle$ is the squared cosine of the angle between the c crystal axis and the drawing direction. $f_c = 1$ means perfect orientation with the drawing direction, $f_c = 0$ for an isotropic sample, and$f_c = -0.5$ for a sample with complete perpendicular orientation with respect to the drawing direction.

$\langle\cos^2\phi_{(hkl),Z}\rangle$, the mean squared cosine of the angle between the normal of a particular crystallographic plane and the stretching direction, can be obtained from the azimuthal intensity distribution, $I(\phi)$, by the following equation:

$$\langle\cos^2\phi_{(hkl),Z}\rangle = \frac{\int_0^{\pi/2} I(\phi)\sin\phi\cos^2\phi d\phi}{\int_0^{\pi/2} I(\phi)\sin\phi d\phi} \tag{5}$$

Ihn et al.[42] have reported that the crystal structure of PBS is monoclinic with unit cell dimensions $a = 0.523$ nm, $b = 0.908$ nm, $c = 1.079$ nm, $\beta = 123.9^\circ$ ($b \perp ac$). Wilchinsky's treatment of uniaxial orientation[43] gives us a commonly used method to measure $\langle\cos^2\phi_{c,Z}\rangle$ by WAXD. Two equations were derived as follows:

$$\begin{aligned}\langle\cos^2\phi_{hkl,Z}\rangle = {} & e^2\langle\cos^2\phi_{X,Z}\rangle + f^2\langle\cos^2\phi_{Y,Z}\rangle + g^2\langle\cos^2\phi_{c,Z}\rangle \\ & + 2ef\langle\cos\phi_{X,Z}\cos\phi_{Y,Z}\rangle + 2fg\langle\cos\phi_{Y,Z}\cos\phi_{c,Z}\rangle \\ & + 2eg\langle\cos\phi_{c,Z}\cos\phi_{X,Z}\rangle \end{aligned} \tag{6}$$

$$\langle\cos^2\phi_{X,Z}\rangle + \langle\cos^2\phi_{Y,Z}\rangle + \langle\cos^2\phi_{c,Z}\rangle = 1 \tag{7}$$

$\cos\phi_{X,Z}$, $\cos\phi_{Y,Z}$, and $\cos\phi_{c,Z}$ as the respective set of director cosines, e, j, and g are the direction cosines of the normal of planes with respect to x, y, and c, respectively.

As the unit cell of PBS crystals is monoclinic, and $b \perp ac$, $\langle\cos\phi_{X,Z}\cos\phi_{Y,Z}\rangle = \langle\cos\phi_{Y,Z}\cos\phi_{c,Z}\rangle = 0$. Furthermore, (0 2 0) and (1 1 0) are two highest diffraction peaks of the infraction curve.

For the (0 2 0) plane, $e = g = 0, f = 1$, eq. (6) can be simplified as follows:

$$\langle\cos^2\phi_{020,Z}\rangle = \langle\cos^2\phi_{Y,Z}\rangle. \tag{8}$$

For (1 1 0) plane, $g = 0, e^2 + f^2 = 1$, eq. (6) can be simplified as follows:

$$\langle\cos^2\phi_{110,Z}\rangle = e^2\langle\cos^2\phi_{X,Z}\rangle + (1-e^2)\langle\cos^2\phi_{Y,Z}\rangle. \tag{9}$$

According to the unit cell dimensions of PBS ($a = 0.523$ nm, $b = 0.908$ nm), $e = 0.867$ can be calculated by trigonometry. Combine eqs. (7)–(9) and the value of e, $\langle\cos^2\phi_{c,Z}\rangle$ of PBS crystals can be calculated as follows:

$$\langle\cos^2\phi_{c,Z}\rangle = 1 - 1.33\langle\cos^2\phi_{110,Z}\rangle - 0.67\langle\cos^2\phi_{020,Z}\rangle \tag{10}$$

To quantify the molecular orientation in the amorphous phase, the Hermans–Stein orientation function [eq. (4)] can be rewritten as[44]:

$$f_{am} = \frac{3\langle\cos^2\phi\rangle - 1}{2} \tag{11}$$

where f_{am} is the amorphous orientation parameter, and φ is the angle between the molecular chain and the drawing direction.

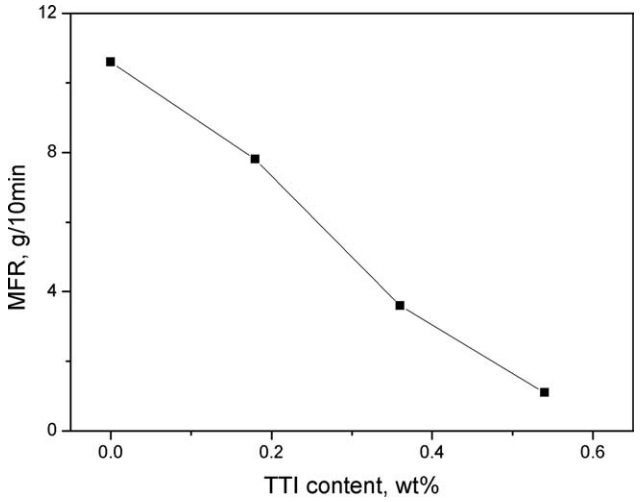

Figure 4. MFR of PPC/35PBS blends with different TTI contents.

Scanning Electron Microscopy Observation

Specimens were prepared by fracturing the films in liquid nitrogen, and the fracture surface was coated with a thin layer of gold, then, the morphology of the films were observed by scanning electron microscopy (SEM; Jeol JSM-6330F).

RESULTS AND DISCUSSION

Preparation and Properties of PPC/PBS Blends

PPC was blended with 35 wt % PBS using varying amounts of TTI as coupling agent. TTI was added at 0, 0.18, 0.36, and 0.54 wt % to the PPC/PBS blends (B1, B2, B3, and B4, respectively). From the results shown in Figure 4, it can be seen that the MFR of the blends decreased with increasing TTI content. When TTI content was 0.54 wt %, MFR changed to 1.1 g/10 min. However, the one without TTI addition was 9.6 g/10 min. This indicated that the molecular weight increased, when TTI was added.

Table III shows the mechanical and thermal properties of PPC/35% PBS blends with different contents of TTI. The tensile strength of the blends improved slightly, but the strain at break increased obviously. The strain at break for the sample with 0.36 wt % TTI was almost five times of the one without TTI addition. This demonstrated that the compatibility between PPC and PBS can be effectively enhanced in the presence of TTI. Also from Table III, the impact strength and Vicat soft temperature of the blends increased with increasing TTI content. In our previous work, we reported the mechanical properties of PPC/PBS blends without in the absence of any coupling agent.[26] By comparison to the past work, the addition of TTI can enhance the mechanical properties of the blends. The tensile strength increases to 27.8 MPa with the addition of 0.36 wt % TTI, whereas it was just about 24 MPa in Pang's work. The optimal content of TTI was found to be 0.36 wt % TTI.

Table III. Mechanical and Thermal Properties of the Blends with Different TTI Contents

Sample	Vicat softening point (°C)	Tensile strength (MPa)	Elongation at break (%)	Impact strength (kJ/m^2)
B1	57.6	26.5	46.3	4.5
B2	63.2	27.2	128.4	7.6
B3	68.7	27.8	212.0	9.0
B4	65.1	27.1	340.1	8.1

Table IV. Mechanical Properties of Calendared Films Prepared at Various Die Temperature

	Die temperature (°C)					
	160	170	180	190	200	210
Tensile strength (MPa)						
MD	43.8	48.7	50.5	52.9	56.0	45.0
TD	19.3	19.4	20.6	22.5	24.4	20.0
Elongation at break (%)						
MD	126.8	153.4	151.8	146.9	152.5	184.7
TD	98.6	116.4	139.5	189.3	203.9	153.4
Tear strength (N/mm)						
MD	72.1	89.8	96.9	89.1	104.5	79.9
TD	157.4	191.7	193.2	200.6	223.2	183.1

Calendaring Condition Investigation

Table II shows the die temperatures for calendaring films, and the mechanical properties of these films are listed in Table IV. It can be seen that the tensile properties and tear properties in both machine direction (MD) and TD increased with the increase of die temperature when temperature was lower than 200°C, but decreased at the die temperature over 210°C. This decrease is believed to result from the decomposition of either PPC or PBS. In this connection, the die temperature was settled at 200°C, and the different speeds of calendar roller are listed in Table V.

Table V. Tensile Properties of Calendared Films with Different Orientation Degrees

	Sample				
	B3-15	B3-20	B3-25	B3-30	B3-35
Roller speed (rpm)	15	20	25	30	35
Degree of orientation					
f_c	0.150	0.174	0.235	0.244	0.247
f_{am}	0.011	0.010	0.012	0.013	0.013
Tensile strength (MPa)					
MD	48.1	51.8	55.4	57.4	60.4
TD	25.2	24.1	23.5	23.7	23.2
Elongation at break (%)					
MD	138.5	127.9	101.5	133.4	143.0
TD	222.5	179.1	203.6	216.8	249.8

B3-35 means calendared film of B3 with the roller speed of 35 rpm.

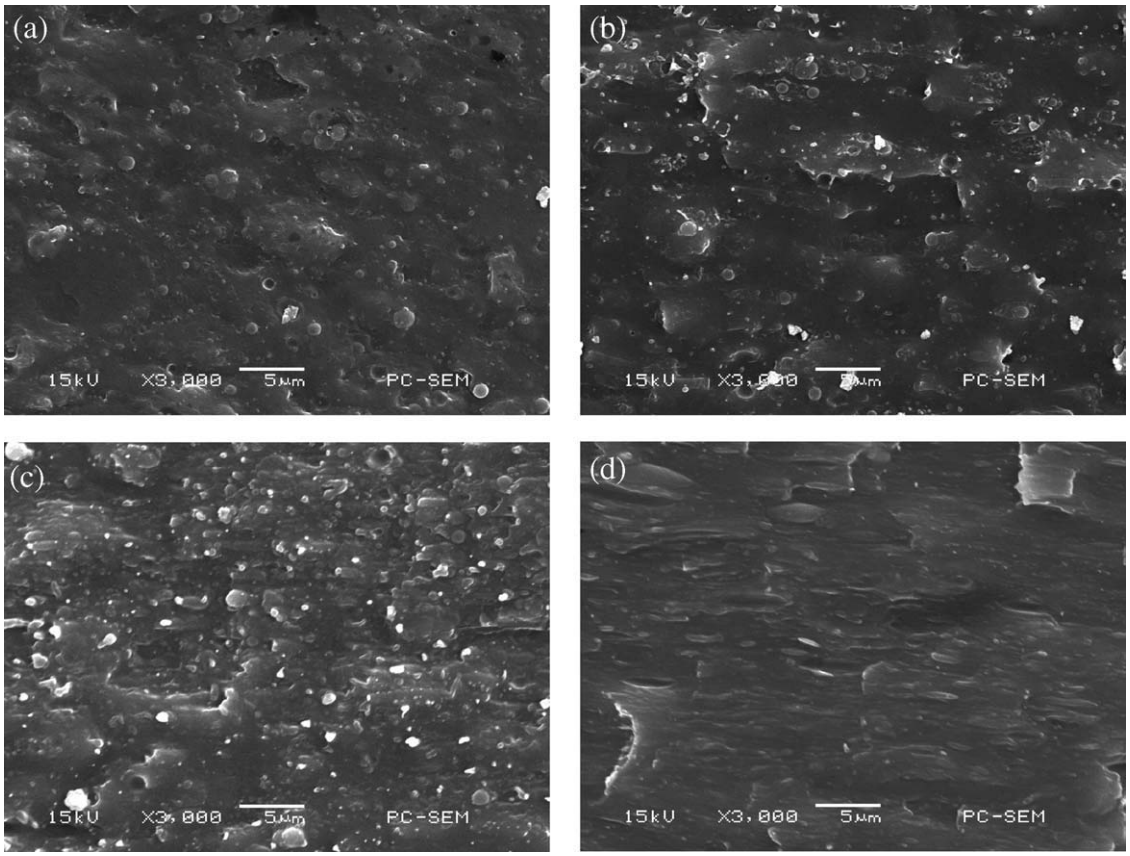

Figure 5. The micrographs in MD direction (a–d correspond to A–D in Fig. 2, respectively).

Morphological of Orientation

There are two stages of orientation process during film formation: the first stage occurred between the die and calendar and the second stage happened when it passed through the gap of nether two rollers. To investigate the orientation of the first stage, the machine was stopped suddenly during film calendaring. Meanwhile, liquid nitrogen was sprinkled on the extruded sheet between the die and the gap of nether two rollers. After cooled down, the sample as shown in vertical view of Figure 2 were obtained and subjected to SEM examination.

The micrographs of A–D sections in MD are shown in Figure 5(a–d). No orientation was detected in both A and B sections, but obvious orientations were observed in both C and D sections. Because of the lower volume fraction and the lower MFR of PBS, the dispersed phases should be PBS. It can be seen that spherical PBS phases were well dispersed within PPC matrix, and they were elongated step by step from C to D sections. The micrographs of final films in MD are shown in Figure 6(b). It can be seen that much higher orientation occurred at second stage. Orientation retraction happened in first stage at high temperature, upon cooling, orientation was retained at second stage of final film, indicating that second stage is critical for orientation.

The different morphology between TD and MD is shown in Figure 6(a, b). Orientation in MD is more obvious than that in TD. Figure 6(c) is an enlarged picture in MD. PBS appeared fibrous shape bestrewed in PPC matrix, with diameter of about 300 nm. The *in situ* fibrillation is believed to contribute a lot to the enhancement of as-made films.

Crystallization Changes

To investigate the crystallinity of the films, the WAXD of PPC, PBS, and their blends were recorded and are shown in Figure 7(a). The neat PBS pattern shows strong peaks at 19.3, 21.7, and 22.4°, which were assigned as (0 2 0), (0 2 1), and (1 1 0) planes, in their turns, and a weak peak of the (1 1 1) plane at 28.7°.[45] These peaks are also found in Figure 7(a) with little deviation, they were at 19.68, 21.62, 22.66, and 29.05° in turn. Upon addition of TTI, all diffraction peaks became weaker, and the crystallinity of the blend reduced from 18.9 to 12.6% when 0.36% TTI was added.

Comparing the WAXD curves of calendared films and PPC/PBS blends in Figure 7(b), the crystallinity of the calendared films were higher than that of PPC/PBS blends. The crystallinity increased with increasing orientation degree. It should notice that the diffraction peak of (0 2 1) in WAXD patterns of films missed due to unclear change on crystal lattice of PBS under highly stretch.

Improvement in Thermal Stability

It is well known that the increase in crystallinity can lead to the increase of thermal stability. As discussed earlier, orientation generally results in the increase of crystallinity for crystalline

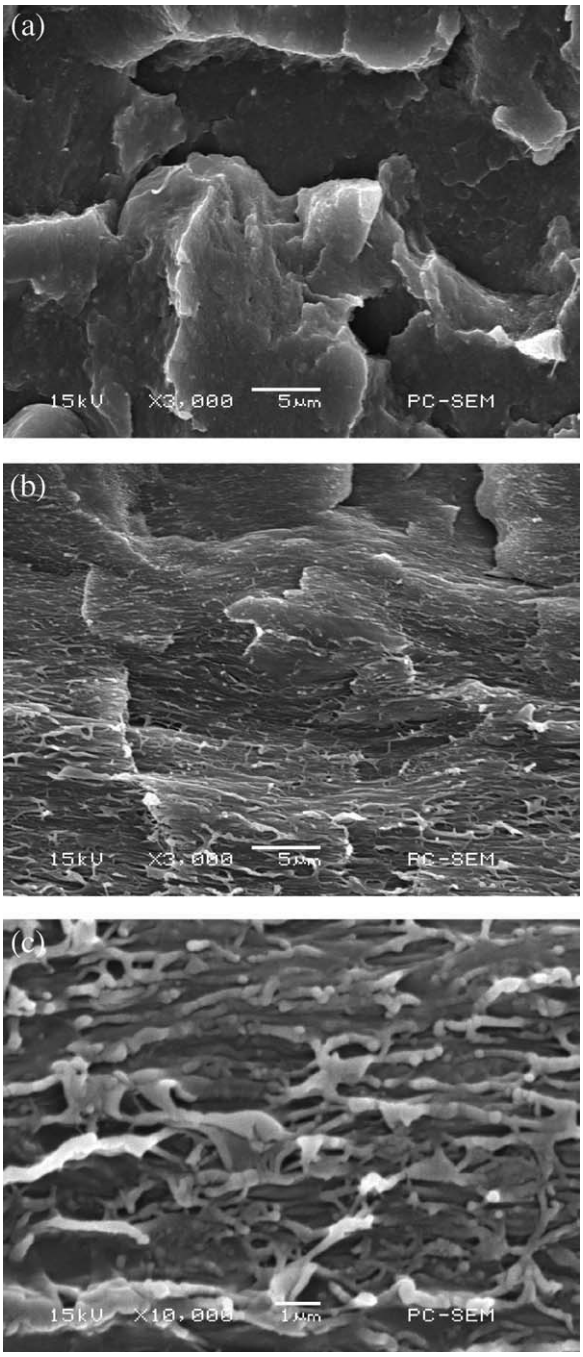

Figure 6. The micrographs of calendared films in different directions: (a) TD, (b) MD, and (c) enlarge view of (b).

polymers. Because of the crystalline nature of PBS, the calendared films of PPC/PBS blends should exhibit better thermal stability.

Figure 8 shows the DSC curves of first and second scan for the film B3-35. It is apparent that the T_g from first scan was 27.1°, whereas that from second scan was 33.8°. The lower T_g from first scan was resulted from the relax of the oriented amorphous phases. The crystallization peak became very apparent in the first scan compared to the blend without orientation. Similarly, two molten peaks at 104.5 and 113.3°C were observed in second

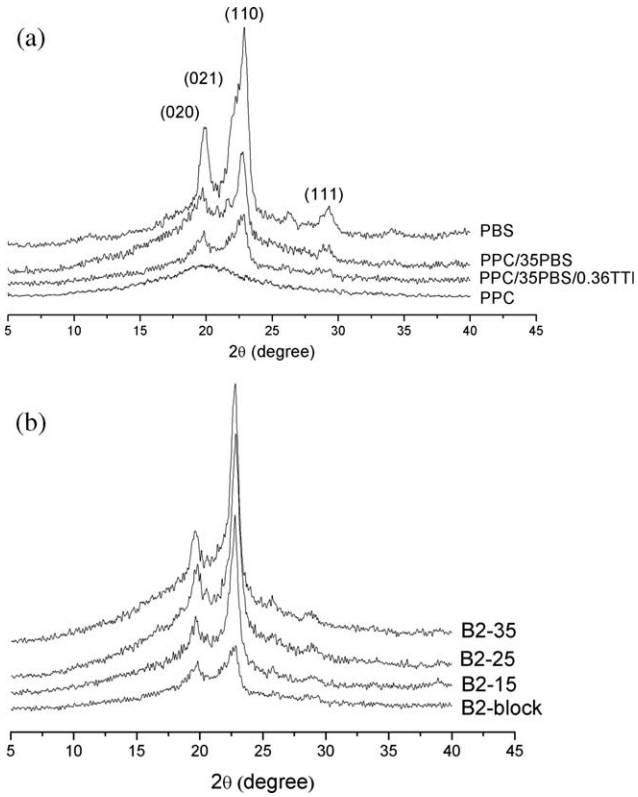

Figure 7. WAXD of PPC, PBS, blend, and films: (a) PPC, PBS, and their blends and (b) films with different orientation degrees.

scan, revealing the incomplete crystallization of PBS during film calendaring. The melting enthalpies in first and second heating were 26.71 and 18.61 J/g, respectively, demonstrating the higher crystallinity of PBS in calendared film. The improved thermal stability data are given in Table VI.

Orientation Characterization

To avoid the influence of crystallographic peak, the saddle with 2θ of 20.6° was chosen to investigate the degree of orientation

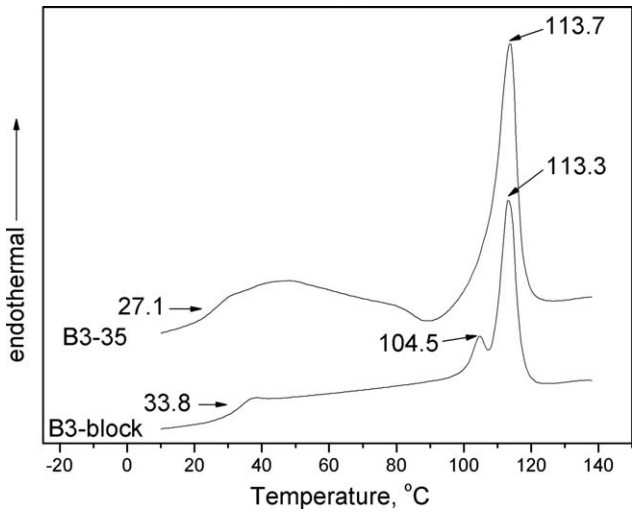

Figure 8. DSC curve of calendared films.

Table VI. Thermal Properties of Calendared Films

Sample	Second heating	First heating		
		B3-15	B3-25	B3-35
T_g (PPC) (°C)	33.8	27.2	26.8	26.7
T_m (°C)	104.5, 113.3	113.3	113.7	113.7
ΔH_m (J/g)	18.61	22.08	24.59	26.71

in amorphous phase. (0 2 0) and (1 1 0) planes of PBS reflection were azimuthally scanned at $2\theta = 19.7$ and 22.7°, and the scanning angle ranges from −90 to 90°. Figure 9 shows radical scan curve of B-35 at three different 2θ values. The exhibition of peaks indicated the existence of the orientation in both crystal and amorphous region. The full width at half maximum (FWHM) has linear relationship with the degree of orientation. The degree of orientation increases with increasing FWHM. The degree of orientation, which can be calculated from the data of radical scan and eqs. (4), (5), (10), and (11), is given in Table V. The degree of orientation of both crystal and amorphous increased with increasing roller speed. Moreover, the orientation of amorphous phase was much smaller than crystalline region. Presumably, the oriented molecular chain of amorphous phase reverted back after being calendared owing to its low T_g of PPC. From the degree of orientation, we can see that the enhancement in mechanical properties mainly depend on the orientation degree of PBS crystalline region.

Mechanical Properties of Calendared Film

Due to the orientation, the mechanical properties of calendared films were different in TD and MD sections. As shown in Table V, the tensile strength in MD section was much higher than that in TD. Moreover, the tensile strength in MD section increased sharply with increasing the degree of orientation. The tensile strength in MD section reached 60.4 MPa when the degree of orientation for PBS crystals was 0.247.

Figure 10 shows the stress–strain curves in both TD and MD sections. The stress decreased after yield point in TD section, while exhibited a hard elastic behavior in MD section. The

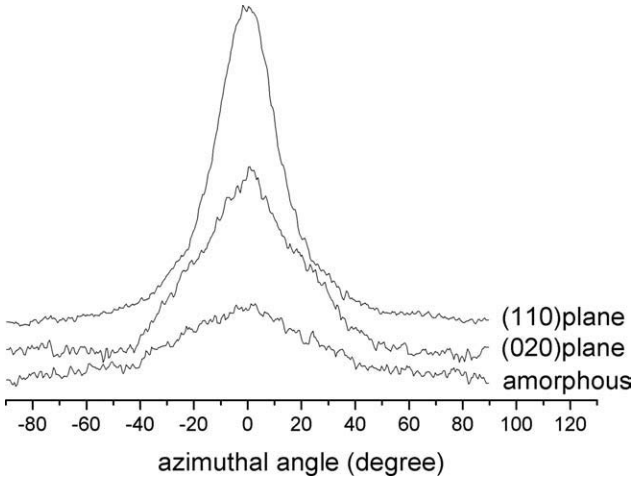

Figure 9. Radical scan of amorphous and crystalline plane.

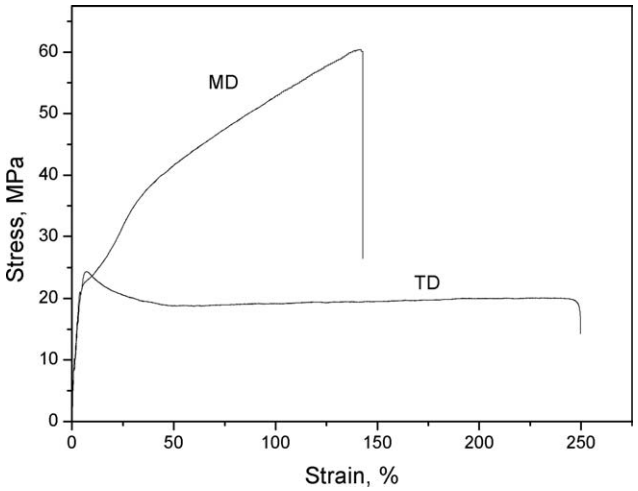

Figure 10. Stress–strain curves in TD and MD directions.

stress increased continuously with increasing strain because of the well-oriented structure of the film. In TD section, the stress–strain behavior was similar with PPC/PBS blend due to the lower degree of orientation of the film.

Two methods were used to investigate the tear properties of the films, namely, Graves tear test and essential work of fracture test. The tear strength obtained from Graves tear testing is listed in Table VII. Contrary to tensile strength, the tear strength in TD direction increased with increasing degree of orientation, whereas it decreased in MD direction. All samples had superior tear properties compared to commercial PE film.

Figure 11 depicts the load–displacement curves of MD and TD directions for B2-35 sample. Both the maximum load and the maximum displacement increased with increasing ligament size. Hence, the total work of fracture, which is calculated as the area under the curve, increased accordingly. Meanwhile, both maximum load and maximum elongation of TD direction were higher than those of MD direction.

To describe the overall tear performance of films, two important factors should be considered, that is, the intrinsic tear resistance, which can indicate the initiation of tear, and the

Table VII. Tear Properties of Calendared Films

	Sample				
	B3-15	B3-20	B3-25	B3-30	B3-35
Graves tear (N/mm)					
MD	122.3	116.4	105.8	102.6	98.4
TD	193.9	201.1	214.2	222.5	230.1
EWF (kJ/m^3)					
MD	33.9	32.4	28.6	27.7	24.7
TD	49.8	53.9	55.3	59.4	63.6
Slope (MJ/m^3)					
MD	4.8	4.5	4.1	3.6	3.3
TD	11.4	12.6	13.9	14.6	16.1

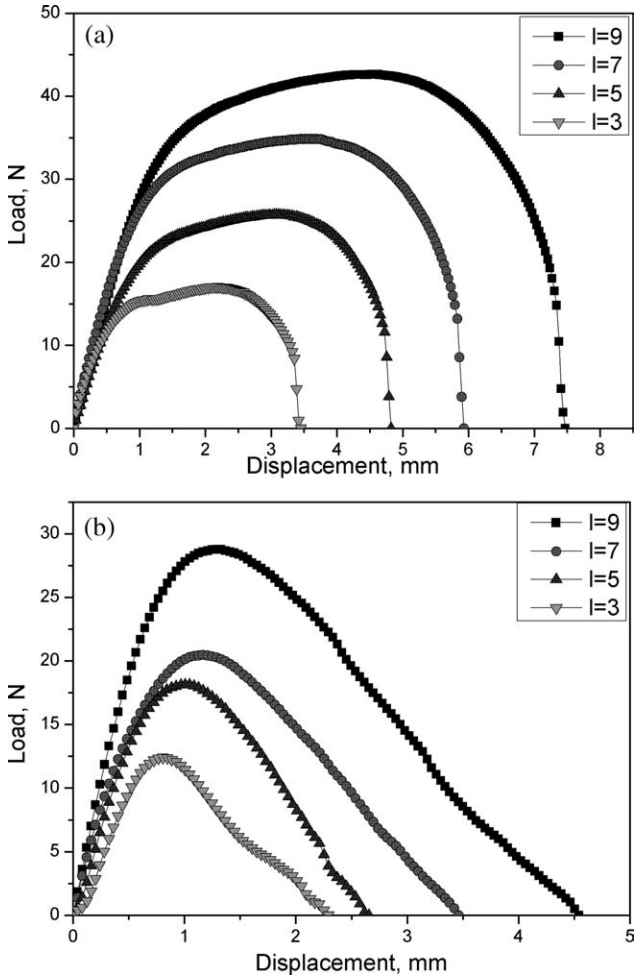

Figure 11. Load–displacement curves from EWF tests: (a) TD direction and (b) MD direction.

formation of microcrazes or voids in the process zone in front of a crack tip. Choi[46] established the relationship between tear performance and EWF data. According to this theory, the

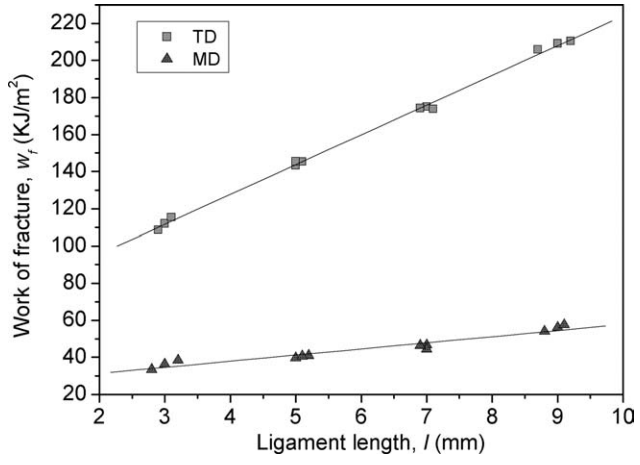

Figure 12. Energy–ligament curves for TD and MD cracks of B3-35 sample.

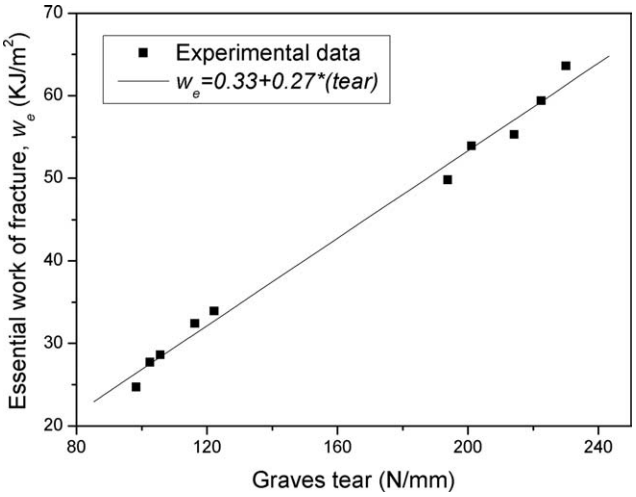

Figure 13. The relationship between EWF and Graves tear strength.

intrinsic tear resistance and whitening zone effect can be explained by EWF and non-essential work of fracture (NEWF), respectively. The former is the *y*-intercept of the fitted curve of the energy–ligament diagram, and the latter is the slope of the energy–ligament curve.

The energy–ligament curves are shown in Figure 12 for TD and MD cracks, and the EWF test results are listed in Table VI. A well-linear relationship between EWF data and orientation degree can be seen in Figure 12. Both EWF and slope increased with increasing orientation degree of TD direction, while decreased of MD direction. Both Graves tear strength and EWF data showed similar results. A well-correlated relationship between Graves tear strength and EWF data are showed in Figure 13.

CONCLUSIONS

TTI was found to be an effective reactive compatibilizer for the melt blending of PPC and PBS. The optimal mechanical properties of the blend were obtained using 0.36 wt % TTI. Uniaxial orientation films of PPC/30%PBS blend can be readily prepared by calendaring process. The optimized processing conditions are die temperature of 200°C and screw speed of 70 rpm. The orientation can in turn enhance both tensile and tear strengths of the as-made films. The *in situ* formation of PBS fibrils well dispersed within PPC matrix is believed the main contribution of this enhancement. Moreover, the increase in the crystallinity of PBS phase within the blend can also improve the mechanical strength and thermal stability of the films. Finally, the as-made films exhibited better mechanical strength in MD section compared with that in TD section. The highest tensile strength in MD section and tear strength of TD direction were 60.4 MPa and 230.1 N/mm, respectively, in case that the degree of orientation was 0.247.

ACKNOWLEDGMENTS

The authors thank the China High-Tech Development 863 Program (2009AA034900 and 2009AA03Z340), Guangdong Province Universities and Colleges Pearl River Scholar Funded Scheme (2010), Guangdong Province Sci & Tech Bureau (Key Strategic

Project Grant Nos. 2008A080800024 and 10151027501000096), and Chinese Universities Basic Research Founding for financial support of this work.

REFERENCES

1. Bugoni, L.; Krause, L.; Virginia, P. M. *Mar. Pollut. Bull.* **2001,** *42*, 1330.
2. Yang, F.; Murugan, R.; Wang, S.; Ramakrishna, S. *Biomaterials* **2005,** *26*, 2603.
3. Martin, O.; Avérous, L. *Polymer* **2001,** *42*, 6209.
4. Mikos, A. G.; Thorsen, A. J.; Czerwonka, L. A.; Bao, Y.; Langer, R.; Winslow, D. N.; Vacanti, J. P. *Polymer* **1994,** *35*, 1068.
5. Ferreira, B. M. P.; Zavaglia, C. A. C.; Duek, E. A. R. *J. Appl. Polym Sci.* **2002,** *86*, 2898.
6. Gan, Z. H.; Abe, H.; Kurokawa, H.; Doi, Y. *Biomacromolecules* **2001,** *2*, 605.
7. Lyoo, W. S.; Kim, J. H.; Yoon, W. S.; Ji, B. C.; Choi, J. H.; Cho, J.; Lee, J.; Yang, S. B.; Yoo, Y. *Polymer* **2000,** *41*, 9055.
8. Tsutomu, O.; Lee, S. H. *J. Appl. Polym. Sci.* **2005,** *97*, 1107.
9. Broecker, W. S. *Science* **1997,** *278*, 1582.
10. Meehl, G. A. *Nature* **1996,** *382*, 56.
11. Kacholia, K.; Reck, R. A. *Climate Change* **1997,** *35*, 53.
12. Inoue, S.; Koinuma, H.; Tsurata, T. *J. Polym. Sci. Polym. Lett. Ed.* **1969,** *7*, 287.
13. Nishimura, M.; Kasai, M.; Tsuchida, E. *Makromol. Chem.* **1978,** *179*, 1913.
14. Guan, H. L.; Xie, Z. G.; Tang, Z. H.; Xu, X. Y.; Chen, X. S.; Jing, X. B. *Polymer* **2005,** *46*, 2817.
15. Chisholm, M. H.; Navarro-Llobet, D.; Zhou, Z. P. *Macromolecules* **2002,** *35*, 6494.
16. Ree, M.; Bae, J. Y.; Jung, J. H.; Shin, T. J. *J. Polym. Sci. Part A: Polym. Chem.* **1999,** *37*, 1863.
17. Meng, Y. Z.; Du, L. C.; Tjong, S. C.; Zhu, Q.; Hay, A. S. *J. Polym. Sci. Part A: Polym. Chem.* **2002,** *40*, 3579.
18. Wang, S. J.; Tjong, S. C.; Du, L. C.; Zhao, X. S.; Meng, Y. Z. *J. Appl. Polym. Sci.* **2002,** *85*, 2327.
19. Zhu, Q.; Meng, Y. Z.; Tjong, S. C.; Zhao, X. S.; Chen, Y. L. *Polym. Int.* **2002,** *51*, 1079.
20. Ge, X. C.; Xu, Y.; Meng, Y. Z.; Li, R. K. Y. *Compos. Sci. Technol.* **2005,** *65*, 2219.
21. Xu, J.; Li, R. K. Y.; Xu, Y.; Meng, Y. Z. *Eur. Polym. J.* **2005,** *41*, 881.
22. Qiu, F. R.; Chen, S. M.; Tan, L.; Ping, Z. H. *Polymer* **2004,** *45*, 3045.
23. Jiao, J.; Wang, S. J.; Xiao, M.; Xu, Y.; Meng, Y. Z. *Polym. Eng. Sci.* **2007,** *47*, 174.
24. Wang, X. L.; Du, F. G.; Meng, Y. Z.; Li, R. K. Y. *Mater. Lett.* **2006,** *60*, 509.
25. Tsutomu, O.; Lee, S. H. *J. Appl. Polym. Sci.* **2005,** *97*, 1107.
26. Pang, M. Z.; Qiao, J. J.; Jiao, J.; Wang, S. J.; Xiao, M.; Meng, Y. Z. *J. Appl. Polym. Sci.* **2008,** *107*, 2854.
27. Kylmä, J.; Seppälä, J. V. *Macromolecules* **1997,** *30*, 2876.
28. Stolt, M.; Hiltunen, K.; Södergård, A. *Biomacromolecules* **2001,** *2*, 1243.
29. Zeng, J. B.; Li, Y. D.; Zhu, Q. Y.; Yang, K. K.; Wang, X. L.; Wang, Y. Z. *Polymer* **2009,** *50*, 1178.
30. Harada, M.; Ohya, T.; Iida, K.; Hayashi, H.; Hirano, K.; Fukuda1, H. *J. Appl. Polym. Sci.* **2007,** *106*, 1813.
31. Broberg, K. B. *J. Mech. Phys. Solids* **1971,** *19*, 407.
32. Broberg, K. B. *J. Mech. Phys. Solids* **1975,** *23*, 215.
33. Cotterell, B.; Reddel, J. K. *Int. J. Fract.* **1977,** *13*, 267.
34. Mai, Y. W.; Cotterell, B. *Int. J. Fract.* **1986,** *32*, 105.
35. Mai, Y. W.; Cotterell, B.; Horlyck, R.; Vigna, G. *Polym. Eng. Sci.* **1987,** *27*, 804.
36. Karger-Kocsis, J.; Czigány, T.; Moskala, E. J. *Polymer,* **1998,** *39*, 3939.
37. Karger-Kocsis, J.; Czigány, T. *Polymer* **1996,** *37*, 2433.
38. Poon, W. K. Y.; Ching, E. C. Y.; Cheng, C. Y.; Li, R. K. Y. *Polym. Test.* **2001,** *20*, 395.
39. Levita, G.; Parisl, L.; Mcloughlin, S. *J. Mater. Sci.* **1996,** *31*, 1545.
40. Hashemi, S. *J. Mater. Sci.* **1997,** *32*, 1563.
41. Stein, R. S. *J. Polym. Sci.* **1958,** *31*, 327.
42. Ihn, K. J.; Yoo, E. S.; Im, S. S. *Macromolecules* **1995,** *28*, 2460.
43. Wilchinsky, Z. W. Advances in X-ray Analysis, Vol. *6*; Plenum Press: New York, **1963, p 231.**
44. Trottier, A. M.; Zwanziger, J. W.; Murthy, N. S. *J. Appl. Polym. Sci.* **2008,** *108*, 4047.
45. Park, J. W.; Kim, D. K.; Im, S. S. *Polym. Int.* **2002,** *51*, 239.
46. Choi, B.-H.; Demirors, M.; Patel, R. M.; deGroot, A. W.; Anderson, K. W.; Juarez, V. *Polymer* **2010,** *51*, 2732.